Computational Parametric Study of the Axial and Radial Clearances in a Centrifugal Rotary Blood Pump

Article *in* ASAIO Journal · October 2017

DOI: 10.1097/MAT.0000000000000700

5 authors, including:

Mohammad Amin Rezaienia
Queen Mary, University of London
22 PUBLICATIONS **69** CITATIONS
SEE PROFILE

Gordon Paul
Queen Mary, University of London
21 PUBLICATIONS **83** CITATIONS
SEE PROFILE

Eldad Avital
Queen Mary, University of London
113 PUBLICATIONS **545** CITATIONS
SEE PROFILE

Martin Rothman
William Harvey Research Institute
187 PUBLICATIONS **2,753** CITATIONS
SEE PROFILE

Computational Parametric Study of the Axial and Radial Clearances in a Centrifugal Rotary Blood Pump

M. A. Rezaienia[a], G. Paul[a], E. J. Avital[a], M. Rothman[b], T. Korakianitis[c*]

[a]School of Engineering and Materials Science, Queen Mary University of London, Mile End Road, E1 4NS, UK
[b]Department of Cardiology, London Chest Hospital, Barts and the London NHS Trust, London, UK
[c]Parks College of Engineering, Aviation and Technology, Saint Louis University, St. Louis, Missouri 63103, USA

Abstract

In centrifugal Rotary Blood Pumps (RBP), clearances are a critical parameter in determining blood trauma. This study investigates the effect of axial clearance (C_{ax}) and radial clearance (C_{rad}) on the hydrodynamic and haemolytic performance of a centrifugal RBP. A centrifugal pump was parameterised so that it could be defined by geometric variables C_{ax} and C_{rad}. Optimal Latin Hypercube Sampling was used to determine design points based on C_{ax}, C_{rad} and rotor speed (ω). For each design point, a computational simulation was conducted to determine efficiency (η) and Normalised Index of Haemolysis (NIH). Next, a Response Surface (RS) was created to estimate these performance parameters based on the design variables. The results show that for a given C_{ax}, when C_{rad} is decreased, η increases until C_{rad} = 0.15 mm, beyond which η deceases. For a given C_{rad}, C_{ax} has a unimodal relationship with η. NIH has a unimodal relationship with both C_{ax} and C_{rad}. The mechanisms behind these relationships were investigated by various analytical methods. It was found that vortices in the secondary flow paths were a critical factor in determining efficiency and haemolysis. The optimal clearance values discerned in this study are only valid for the specific impeller geometry and operating conditions analysed.

Keywords: VAD, MCS, CFD, Haemolysis, Clearance, CHF, Rotary blood pump, Centrifugal

Nomenclature

Subscripts:

ax	axial
down	down
exp	exposure
max	maximum
min	minimum
out	outlet
rad	radial
tot	total
up	up

Abbreviations and Acronyms:

2-D	Two Dimensional
3-D	Three Dimensional
C	Clearance
CAD	Computer Aided Design
CHF	Congestive Heart Failure
CFD	Computational Fluid Dynamic
F	Force
HB	Total Blood Haemoglobin
LHS	Latin Hypercube Sampling
MRF	Multi Reference Frame
NIH	Normalised Index of Haemolysis
P	Pressure
pfhb	plasma free haemoglobin
Q	Flow Rate
R	Resistance
RS	Response Surface
RBP	Rotary Blood Pump
RBC	Red Blood Cell
Re	Reynolds Number
s	second
η	efficiency
ρ	density
μ	viscosity
ω	rotor speed
σ	Von Mises shear stress

Introduction

Congestive Heart Failure (CHF) is one of the leading causes of death in Western countries. More than seven million people in North America and Europe are diagnosed with heart failure, among whom nearly 6% are categorised as having New York Heart Association class IV heart failure[1]. As a result, the role of Rotary Blood Pumps (RBPs) has become vital for patients on and off the waiting list[2,3].

One of the challenges with the traditional RBP devices is their highly invasive implantation procedure which make many elderly and ill patients no longer eligible for the surgery. This has encouraged many research groups to focus on the design and development of miniaturised RBPs, aimed for minimally invasive surgery [4,5,6,7,8,9] Miniaturised RBPs, due to their inherently higher rotor speeds, are more susceptible to shear-induced blood trauma[10]. As a result, in the design and development process of an RBP device, improving the haemolytic performance is of critical importance. Since the non-optimised design of such an RBP may lead to clinical complications such as haemolysis[11], thrombosis[12], bleeding[13] and infection[14].

Haemolysis is an important indicator to evaluate the haemolytic performance of an RBP[15]. Haemolysis is defined as the amount of haemoglobin entering into blood plasma as a result of the mechanical damage of the membranes of Red Blood Cells (RBCs), known as plasma free haemoglobin (pfhb). In the long term, haemolysis may lead to biochemical alterations in blood that can result in reduced life expectancy[16].

One of the key regions inside a rotary centrifugal blood pump, which significantly affects the haemolytic as well as hydrodynamic performance, is the clearance between the impeller and its casing.

Graefe et al.[17] reported that among parameters including length, diameter, clearance, rotor speed, force and pressure, the clearance is the most critical design parameter affecting blood trauma. Kosaka et al[18] showed that as the axial gap in a hydrodynamic bearing was increased from 1 to 63 μm the NIH improved by 95%. Kido et al.[19] showed that changing the clearances from 0.1 to 0.2 mm had a minimal effect on the pump's efficiency yet significantly increased haemolysis. Wu et al.[20] showed that as the radial clearance is reduced from 0.1 mm to 0.05 mm, the efficiency remains relatively constant. They observed that for their low Reynolds number RBP device, as the radial clearance decreases below 0.1 mm viscous effects are more significant than volumetric leakage. James et al.[21], reported that haemolysis varied minimally in the VentrAssist when the running clearance was varied between 0.075 to 0.215 mm. Paul et al.[22] investigated the effect of clearances on the hydrodynamic

characteristics in centrifugal blood pumps and reported that slip and turbulence have a significant effect on the pressure distribution and blood compatibility at small and large clearances respectively.

The range of clearances which are feasible are highly dependent on the bearing mechanism used to stabilise the pump. For example, HVAD and VentrAssist use a passive hydrodynamic bearing, necessitating small clearances[23,24], whereas HeartMate III uses an active magnetic bearing, incorporating relatively large clearances[25].

It is evident from the literature that the clearance affects performance parameters differently in different pump designs, so a methodology is required to evaluate optimal clearances individually for each pump. To our knowledge, the relative and independent effect of axial versus radial clearances has not been investigated.

The aim of this study is to investigate the effect of radial and axial clearance sizes in a centrifugal pump on hydrodynamic and haemolytic parameters, with a focus on the hydrodynamic efficiency and haemolysis. The objective of this work is satisfied by means of Computational Fluid Dynamic (CFD) simulations. In recent years, optimisation combined with CFD techniques have been widely used in RBP research[26,27].

Methodology

CFD Model

For conventional centrifugal pumps such as HVAD[28]and Heartmate III[29], the clearances can be classified as radial and axial. The radial clearances are the cylindrical gaps between the outer circumference of the impeller and the radial wall of the casing, and can be further distinguished into upper and lower radial clearances depending on whether they are above or below the volute. The axial clearances are defined as the gap between top and bottom axial faces of the impeller and the top and bottom of the casing. The axial clearances can be further distinguished as top and bottom axial clearances.

For this study, a 3D CAD model of a centrifugal pump was created using Ansys Design Modeler (Ansys Inc., Canonsburg, PA, USA). The blade and volute geometry was taken from work published by Mozafari et al.[30,31] and remains constant for all clearance geometries. It is assumed that the impeller is radially and axially suspended inside the casing and there is no contact between the impeller and the casing wall. The impeller height and diameter were set at 17 mm and 30 mm. This is approximately based on the impeller sizes of HVAD and Heartmate III although the height was increased slightly to create a more significant radial section in the secondary flow paths.

Figure 1 shows a 2D cross-sectional view of the centrifugal pump model. For this model, a design parametrisation of the clearances was conducted. The upper and lower radial clearance sizes are defined as equal and represented by a single design variable, denoted radial clearance (C_{rad}). Similarly, the top and bottom axial clearance sizes are defined as equal and represented by a single design variable, denoted axial clearance (C_{ax}). The range of impeller clearances sizes was defined based on HVAD and HeartMate III. The minimum axial gap for HVAD, with a hydrodynamic bearing, is 40 microns[24]. The maximum radial gap for HM III, with a magnetic bearing, is 1.0 mm[32]. Lower and upper clearance size limits of 0.1 mm and 1.0 mm respectively were implemented for both C_{rad} and C_{ax}. Clearances below 0.1 mm could not be simulated due to limited computational resources.

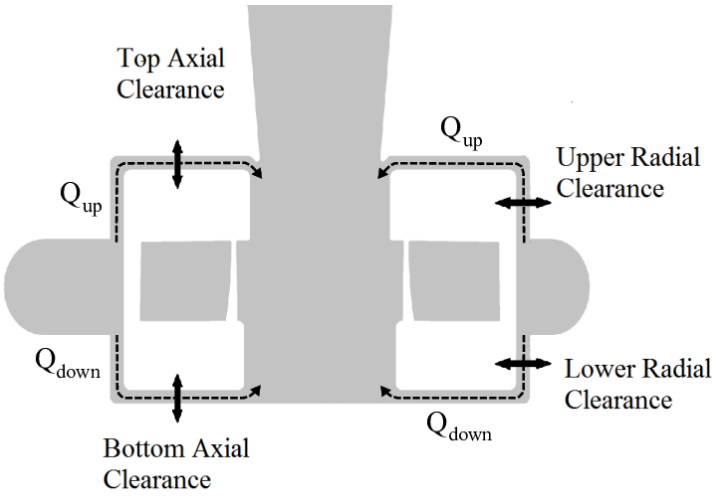

Figure 1: The parameterised CFD model of the pump.

The clearances create paths for secondary flow. As shown in Figure 1, the lower secondary flow rate (Q_{down}) travels downwards from the blade tips to rejoin the main stream from the bottom, while the upper secondary flow rate (Q_{up}) traveling upwards from the blade tips to rejoin the mainstream from the top. Q_{tot} is the sum of Q_{up} and Q_{down}.

A combined tetrahedral, hexahedral and prism element mesh was generated using Ansys mesh tool (Ansys Inc., Canonsburg, PA, USA). The inflation function was used across the surfaces with the near boundary first node of 2^{-5} m. The blood flow was simulated using Ansys CFX (Ansys Inc., Canonsburg, PA, USA). The blood is considered as an incompressible fluid with a viscosity (ϑ) of 0.00035 kg/ms and a density (ρ) of 1050 kg/m3. The boundary conditions were specified as zero total pressure (P) at the inlet and a flow rate (Q_{out}) of 5 L/min at the outlet. For this study, a K- ω (SST) turbulence model was used because of its high accuracy and robustness in the near wall

region[33]. The Multiple Reference Frame (MRF) approach, in which the flow is considered steady state, was used to shorten the computational time. The solution was performed with the convergence target for the velocity and turbulence residuals below 10^{-4}. The simulations were run on a workstation with 16 Intel Xeon quad core 3.2 GHz processors and 64 GB RAM.

Automatic Meshing

One major challenge for automatic meshing in a CFD parametric study is to ensure the quality of the mesh is high enough that the computational results can be considered reliable. In this study, we adopt the methodology used by Thamsen et al.[24] in which the average non-dimensional Y^+ was used as a benchmark to ensure that the Y^+ value is less than 2 for all design cases to ensure the mesh configuration is compatible with the K-ω(SST) model. If any design point exhibits a Y^+ more than 2, the inflation size is corrected accordingly.

Mesh Independence

A clearance configuration consisting of the largest permissible clearances, C_{ax} = C_{rad} = 1.0 mm, was chosen to conduct a mesh dependency study. A mesh with a maximum element size of 1 mm, resulting in 8,141,937 elements, was initially used to solve the simulation. The mesh was then refined by reducing the maximum element size in order to generate a finer mesh and solved again. This process was repeated until there was no significant difference in output achieved by increasing the mesh density. The outlet pressure (P_{out}) was selected as the benchmark. The largest maximum element size which demonstrates mesh independence is used for the parametric and optimisation studies, in which re-meshing for each individual design point is performed automatically.

Haemolysis

Shear-induced haemolysis was computed using the Eulerian-scalar-transport approach, adopted from the studies conducted by Taskin et al.[34]. The scalar transport equation was then expressed as in equation 1.

$$\frac{\mathrm{d}(\Delta \mathrm{HB}')}{\mathrm{dt}} + \mathrm{v}.\rho.\nabla(\Delta \mathrm{HB}') = \mathrm{S} \qquad (1)$$

Where $\Delta \mathrm{HB}'$ is defined as a scalar variable equal to $\Delta \mathrm{HB}^{\frac{1}{\alpha}}$, and $\Delta \mathrm{HB}$ is defined as plasma free haemoglobin, S is the source term defined as $S = \rho(\mathrm{HB}.\mathrm{C}.\sigma^{\beta})^{\frac{1}{\alpha}}$, in which HB is total blood haemoglobin, ρ is the blood density, α, β, and C are constant[34] and σ is defined as Von Mises shear stress, which is calculated from the stress components acting on an RBC membrane as described in equation 2.

$$\sigma = [\frac{1}{6} \sum(\sigma_{ii} - \sigma_{jj})^2 - \sum(\sigma_{ij}\, \sigma_{ij})]^{0.5} \quad (2)$$

The average outlet NIH (g/100l) for each individual case is defined in equation 3 adopted from the study by Carswell et al.[15].

$$\text{NIH} = 100 \times \frac{\Delta \text{HB}}{\text{HB}} \times (1\text{-Hct}) \times \text{k} \quad (3)$$

where Hct is the blood haematocrit and k is the haemoglobin content of blood.

Response Surface

The parametric study was conducted by adopting a surrogate modelling approach using Ansys Design Xplorer (Ansys Inc., Canonsburg, PA, USA) tools. Firstly, a Design of Experiments was created using optimal Latin Hypercube Sampling (LHS). The LHS produces a design space represented numerically by sampling points based on the design variables C_{ax}, C_{rad} and ω. This resulted in 15 sampling points. For each sampling point, geometry creation, mesh generation, pre-CFX analysis, computational solution and post-CFX analysis was conducted. The mean computational time for each sampling point was about five hours. This yielded efficiency (η) and NIH from each sampling point.

A Response Surface (RS) was then calculated by fitting a polynomial curve through the computed variables obtained from the DoE, using the Response Surface tool from Ansys. This allows prediction of performance parameters η and NIH from the design variables for any design within the defined range. The RS was used to estimate the required ω for the desired operating condition of 100 mmHg and 5 L/min for 81 design configurations of C_{ax} and C_{rad} with values for each ranging from 0.1 mm to 1.0 mm in increments of approximately 0.1 mm. For each design configurations, ω was defined as the rotor speed which provided the required operating condition. Increased-accuracy simulations were then run for each of the 81 design configurations at the ω estimated by the RS to obtain more reliable results. Any deviation from the required operating condition is corrected by modifying ω in each increased-accuracy simulation. The performance parameters were extracted for each of the 81 design points and the results were used to populate a 2D 9×9 matrix.

Results

The results from the mesh dependency study showed a variation of less than 3% of the P_{out} between the mesh configurations with maximum element sizes 0.2 and 0.1 mm. Consequently a maximum element size of 0.2 mm was used for all mesh generation in this study.

Figure 2(a,b) show η and NIH across the design space with axial and radial clearance sizes ranging from 0.1 to 1.0 mm for the desired operating condition respectively. Figure 2(a) shows that for a given C_{ax}, when C_{rad} is decreased, η increases yet further reduction in C_{rad} below 0.15 mm leads to a decreased efficiency. For a given C_{rad}, a unimodal relationship between efficiency and C_{ax} is observed. For instance, for the C_{rad} of 0.5 mm, as the C_{ax} decreases from 1.0 to 0.5 mm, the efficiency increases by 3.5%, yet a further reduction in C_{ax} below 0.5 mm leads to a drop in the efficiency. The maximum efficiency of 44.3% occurs when C_{ax} is 0.55 mm and C_{rad} is 0.15 mm. The minimum efficiency of 39.5% occurs when C_{ax} and C_{rad} are 1.0 mm.

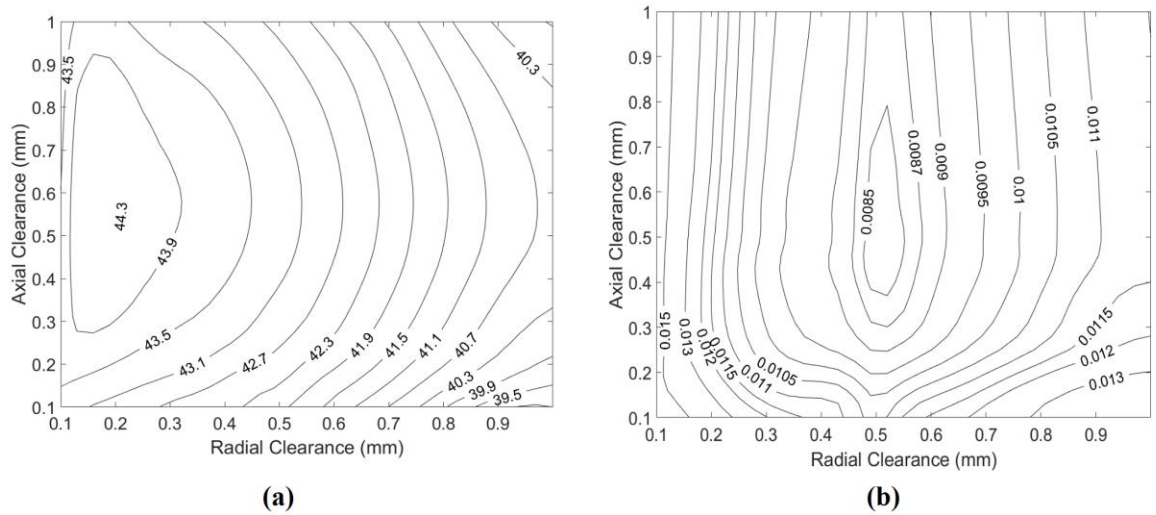

Figure 2:(a) η contours (%) with varying axial and radial clearances for the unique operating condition of 100 mmHg, 5 L/min. (b) NIH contours with varying axial and radial clearances for the unique operating condition of 100 mmHg, 5 L/min.

Figure 2(b) shows that there is a unimodal trend for the effect on NIH of both the radial and axial clearances. For the case where C_{ax} is 0.5 mm, as C_{rad} decreases from 1.0 to 0.55 mm the NIH decreases by 30%, yet further reduction in C_{rad} below 0.55 mm to 0.1 mm leads to an increase of 70% in NIH. The minimum NIH of 0.0081 g/100l occurs where C_{ax} and C_{rad} are 0.55 mm. The maximum NIH of 0.017 g/100l occurs where C_{ax} and C_{rad} are 0.1 mm.

In this study in order to explain the mechanisms behind the observed relationship between clearance sizes and performance parameters, six different design points out of 81 total design points are selected and the local hydrodynamic parameters including shear stress, velocity and secondary flow rates are studied for each individual case.

First the effect of axial clearance was investigated with three axial test cases of $Ax_{0.1}$, $Ax_{0.5}$ and $Ax_{1.0}$ in which C_{rad} is fixed at 0.5 mm and C_{ax} is 0.1 mm, 0.5 mm and 1.0 mm respectively. The ω for these cases were 2600, 2625 and 2620 rpm respectively.

Figure 3 (a,b,c) shows the wall shear stress (WSS) distribution on the bottom axial face of the impeller for these test cases. For case $Ax_{0.1,}$ the bottom axial face has the highest local average WSS of the three cases at 52 Pa. For $Ax_{0.5}$ the local average WSS is 25 Pa, about 50% lower than $Ax_{0.1}$. For case $Ax_{1.0}$ the local average WSS is 32 Pa, about 28% more than $Ax_{0.5}$. The total average WSS across all impeller walls, radial and axial, for the same configurations are 47, 32 and 39 Pa respectively, following the same trend.

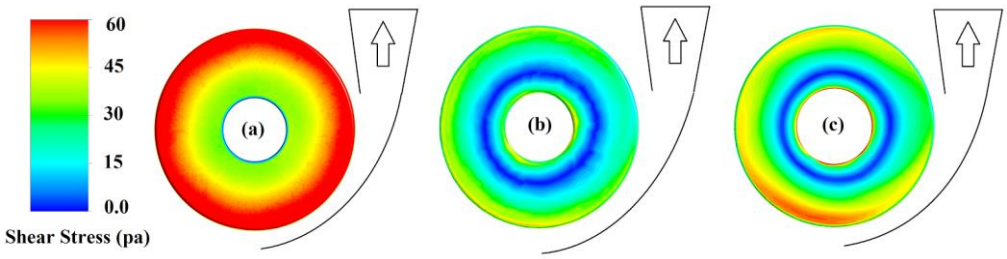

Figure 3: WSS distribution on the bottom axial face of the impellers for the axial test cases (a) Ax0.1, (b) Ax0.5 and (c) Ax1.0 at 100 mmHg, 5 L/min. The volute outlet position is shown on the top right of each pump

Figure 4 (a,b,c) shows the velocity streamlines coloured by shear stress in the bottom axial clearances for the same test cases. For $Ax_{0.1}$ the average σ in the axial clearance is the highest of the three cases at 57 Pa, no recirculating flow is observed in the axial clearance. For $Ax_{0.5}$, the average σ drops by 21% to 45 Pa and some vortices are observed. For $Ax_{1.0}$ the average σ drops to 25 Pa and there are significantly more vortices.

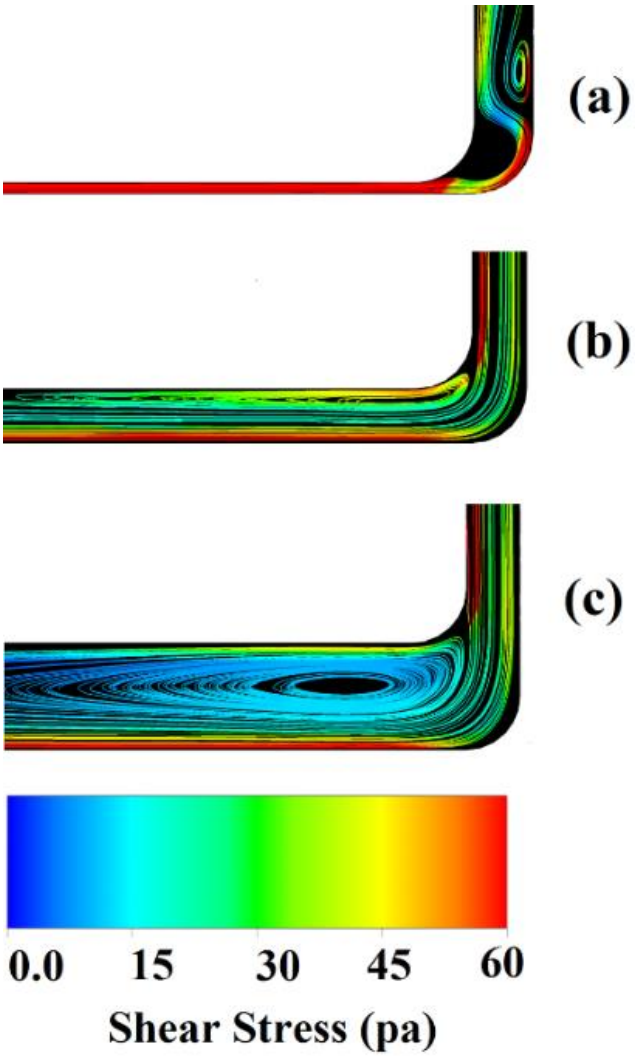

Figure 4: Velocity streamline coloured by shear stress in the bottom axial clearances of (a) Ax0.1, (b) Ax0.5 and (c) Ax1.0 at 100 mmHg, 5 L/min

The upper secondary flow rates (Q_{up}) and lower secondary flow rates (Q_{down}), as illustrated in Figure 1, were recorded for the same cases and presented in Figure 5. Q_{tot} (Q_{up}+Q_{down}) was the highest for $Ax_{0.5}$ and lowest for $Ax_{0.1}$.

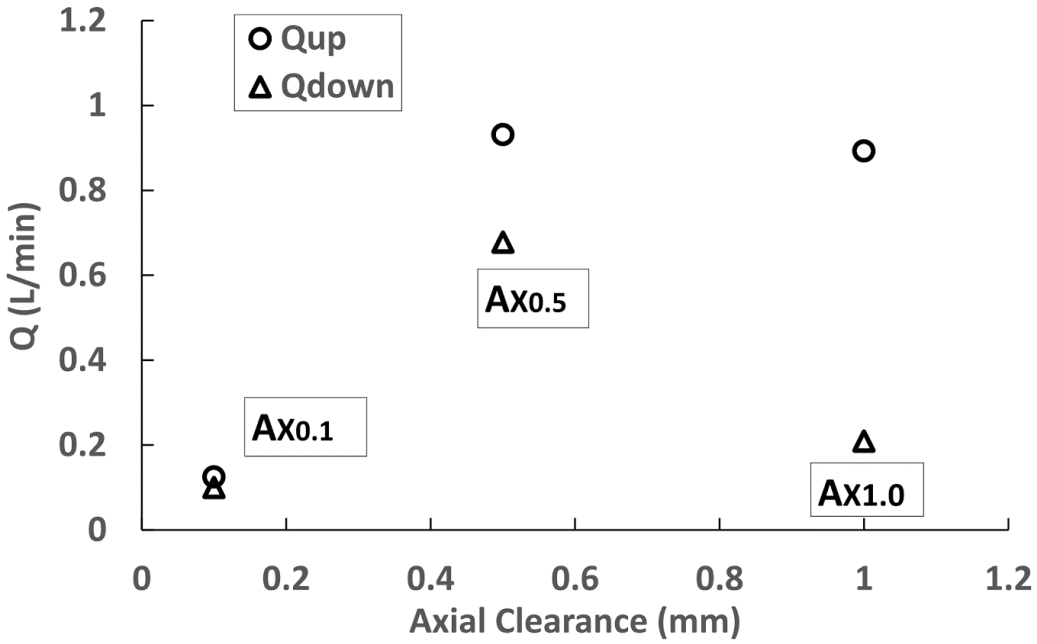

Figure 5: The graphs of secondary flow rate passing through the bottom and top secondary flow paths for the axial test cases Ax0.1, Ax0.5 and Ax1.0 at 100 mmHg, 5 L/min.

Next the effect of radial clearance was investigated with three radial test cases $RAD_{0.1}$, $RAD_{0.5}$ and $RAD_{1.0}$ in which C_{ax} is fixed at 0.5 mm and C_{rad} is 0.1 mm, 0.5 mm and 1.0 mm respectively. The ω for these cases were 2420, 2600 and 2800 rpm respectively.

Figure 6(a) shows the NIH distribution in all flow paths for the three radial test cases of $RAD_{0.1}$, $RAD_{0.5}$ and $RAD_{1.0}$. In all three cases, the highest haemolysis is observed in the bottom and the top axial clearances from which the damaged blood re-enters the primary flow path. For $RAD_{0.1}$, the average outlet NIH is 0.015 g/100l and the maximum NIH appearing in the radial clearances is 0.058 g/100l. For $RAD_{0.5}$ the average outlet NIH is 0.0083 g/100l and the maximum NIH appearing in the radial clearance is 0.032 g/100l, both lower than $RAD_{0.1}$. For $RAD_{1.0}$, the outlet average NIH is 0.011 g/100l and the maximum NIH appearing in the radial clearance 0.041 g/100l is, slightly higher than $RAD_{0.5}$ but lower than $RAD_{0.1}$.

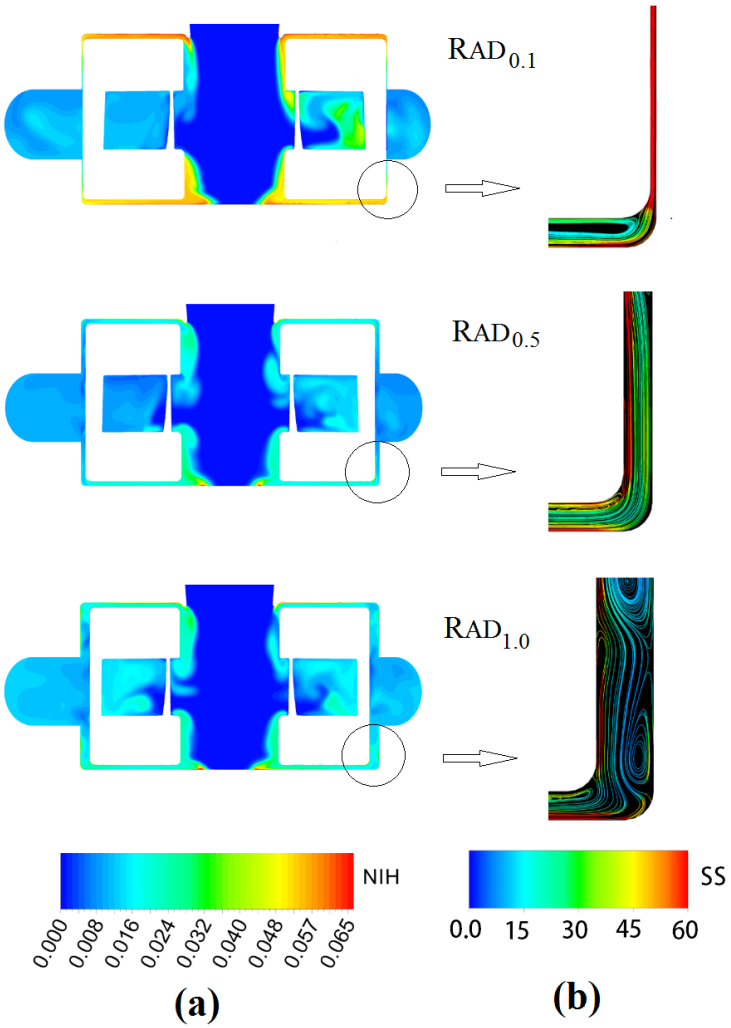

Figure 6: The graphs of secondary flow rate passing through the bottom and top secondary flow paths for the axial test cases Ax0.1, Ax0.5 and Ax1.0 at 100 mmHg, 5 L/min.

Figure 6(b) shows the velocity streamlines coloured by shear stress in the lower radial clearances for the same test cases. For $RAD_{0.1}$ the average σ in the radial clearance is 60 Pa, however no recirculating flow can be observed. For $RAD_{0.5}$ the average σ drops by 16% to 50 Pa. For $RAD_{1.0}$ the average σ in the clearance region drops by 40% to 30 Pa and there are significantly more vortices.

The secondary flow rates were recorded for the same cases and presented in Figure 7. For these cases, the Q_{up} and Q_{down} increased as C_{rad} increased. Q_{tot} was the highest for $RAD_{1.0}$ and lowest for $RAD_{0.1}$.

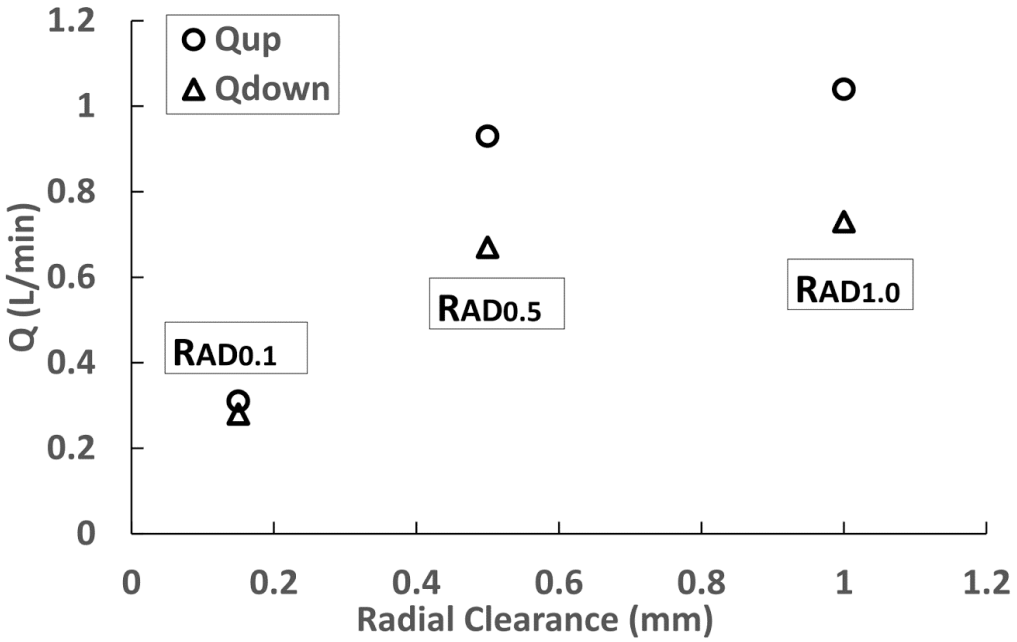

Figure 7: The graphs of secondary flow rate passing through the bottom and top secondary flow paths for the radial test cases (a) RAD0.1, (b) RAD0.5 and (c) RAD1.0 at 100 mmHg, 5 L/min.

The maximum efficiency, minimum efficiency, maximum NIH, minimum NIH were extracted from the 9×9 matrix to further illustrate the effect of clearances on the output parameters. The cases and their performance parameters are summarised in Table 1.

Table 1: Optimized geometrical parameters for a given operating condition of 5 L/min-100 mmHg, aiming at the max efficiency, minimum efficiency, maximum NIH, minimum NIH.

	Param	**C_{ax}**	**C_{rad}**	**Speed**	η	**NIH**	**Q_{up}**	**Q_{down}**	**Q_{tot}**
-	Units	mm	mm	rpm	%	g/100l	l/min	l/min	l/min
1	η_{max}	0.55	0.15	2500	44.3	0.0144	0.54	0.46	1
2	η_{min}	1	1	2800	39.5	0.0115	1	0.14	1.14
3	NIH_{max}	0.1	0.1	2450	43.0	0.0172	0.19	0.13	0.32
4	NIH_{min}	0.55	0.55	2600	42.5	0.0081	0.95	0.7	1.65

Discussion

As reported in previous studies[17,18,19,20,21,22] one of the key challenges in the design and development of an RBP device is the optimisation of clearance sizes. In this study we used a coupled CFD optimisation technique to investigate the hydrodynamic and haemolytic responses of a centrifugal pump with different clearance configurations for a unique operating condition.

Figure 2 shows that C_{ax} and C_{rad} have different effects on the efficiency. For a fixed axial clearance of 0.55 mm, the efficiency shows a proportional relationship with the radial clearance until C_{rad} = 0.15 mm. This is mainly because a reduction in the radial clearance results in less secondary flow, causing hydraulic efficiency to rise. However, this effect appears to be reversed as the radial clearance is reduced below C_{rad} = 0.15 mm. It appears that for C_{rad} less than 0.15 mm, an improved efficiency resulting from reduction in secondary flow are now offset by efficiency degradation resulting from increased viscous friction. This phenomenon was also observed in the report by Wu et al.[20].

The unimodal effect of efficiency with the change in axial clearance can be described by studying the design points of $AX_{0.1}$, $AX_{0.5}$ and $AX_{1.0}$ in Figure 4 and 5. The average shear stress on the bottom axial face is high for

$Ax_{0.1}$, as shown Figure 4(a), meaning more power is required to drive the pump. For case $Ax_{0.5}$, the shear stress is far lower because shear stress is inversely proportional to clearance size where flow is laminar[35]. For case $Ax_{1.0}$, however, large vortices can be observed in Figure 5(c), the flow is no longer laminar and shear stress is high due to the near wall large scale vortices[36,37] which inversely affect the efficiency.

By incorporating the effects of σ and t_{exp}, using equation 1, the NIH was calculated for different configurations of the axial and radial clearances. The results showed that both C_{ax} and C_{rad} have a unimodal relationship with NIH. However, since the level of shear stress on the fluid in the radial clearance is greater than that in the axial clearance due to the higher tangential velocity, the effect of radial clearance on haemolysis is more significant when the axial clearance is greater than 0.3 mm. Below 0.3 mm, high levels of shear stress on the fluid in the axial clearance contribute more significantly to haemolysis. The unimodal relationship between the haemolysis and radial clearances has been reported in the study by Wu et al.[20]. They reported that incorporating very small radial clearances may increase the risk of RBC damage due to excessive shear stress, while large clearances can cause high exposure time.

The unimodal effect of the haemolysis with the axial clearance can be explained by examining the design points of $AX_{0.1}$, $AX_{0.5}$, and $AX_{1.0}$ in Figures 5, 6. As shown in Figure 6, Q_{tot} is the highest at $Ax_{0.5}$, the lowest at $Ax_{0.1}$ due to increased resistance, and lower at $Ax_{1.0}$ due to vortices forming in the bottom axial clearance and illustrated in Figure 5(c). At $Ax_{0.1}$ there is high shear stress on the fluid and the resulting haemolysis is high. At $Ax_{0.5}$ the shear stress is lower. The Q_{tot} is high so the RBC exposure time is not increased. This results in reduced haemolysis. At $Ax_{1.0}$, as shown in Figure 5(c), large vortices are formed in the bottom axial clearance. This results in a significant drop in Q_{down}, as shown in Figure 6. A decreased Q_{down}, due to the vortices, leads to an increased RBC exposure time, and consequently leads to an increased haemolysis[38]. The appearance of large scale stagnant vortices in clearance regions may also lead to impeller instability[39]. In addition, the stagnant vortices may increase the risk of platelet activation which results in thrombosis formation[40].

The design points optimised for various objectives shown in Table 1 give further insight into the effect of clearance on these performance parameters. In Table 1, the maximum efficiency was achieved when C_{rad} was minimised at 0.15 mm but C_{ax} was 0.55 mm. In this theoretical device the fluid resistance in the axial clearances is higher than in the radial clearances for a given Cax = Crad. Consequently C_{ax} should be larger than Crad to prevent vortices.

In Table 1, the maximum NIH occurred at the minimum clearance, but the minimum NIH did not occur at the maximum clearance. The minimum Q_{tot} is observed in the case of maximum NIH, where the clearances are both 0.1 mm. This is not the most efficient design because an RBP is a low Reynolds number pump, in which viscous effects are significant at low clearances and reduce pump efficiency. The detrimental effect on efficiency of high viscous drag is more significant than the positive effect on efficiency of minimising secondary flow at small clearances. The reverse is true at large clearances, where viscous drag is much lower.

Limitations

The geometry of the pump was defined based on literature sources. The result from this study is only valid for this design specification under the defined operating conditions, however the methodology is valid for any centrifugal blood pump.

For the present study, due to the available computational resources, it was not feasible to reduce the clearance size to less than 0.1 mm. However, the range tested appears to capture the optimal design point for NIH and η for the case study in this paper.

No experimental study has been conducted. In computational studies errors may arise associated with turbulence model and mesh quality. These potential confounders were mitigated with the implementation of a highly accurate k-ω SST model and a mesh dependency study respectively. Further, as shown in previous studies[15], there was always a discrepancy between the power law predicted and the measured haemolysis indices. In addition, in this study, it is assumed that the empirical constants of α, β, and C, used in the power law equation, remain unchanged for various clearance configurations. It must be noted that these constants, in many previous studies[34], were determined using Couette-type shearing devices which incorporate a very small gap (<100μm) to ensure that the blood flow regime remains laminar. However, as shown in this study, for large clearances (>0.5mm), the flow regime is fully turbulent. Turbulent flow, due to its inherent excessive stress, may result in further deviation in the predicted haemolysis using the adopted empirical constants[34] and thus may undermine the unimodal haemolysis relationship extracted from simulation results in this work obtained in this study. Therefore, further experimental studies are required to investigate the effect of turbulent flow in large clearances on the haemolysis and tuning the empirical constants of α, β, and C accordingly. It should also be noted that for this study the effect of the surface roughness on haemolysis was not considered.

The model does not account for the haemolysis caused by the bearing design. Hydrodynamic wedge bearings, such as those used in HVAD and VentrAssist[23,24], will have more complex effects on haemolysis. In this paper, to limit the scope, we assume all surfaces are flat and the pump is suspended by other means. One interpretation of this is that small clearances might in fact have higher haemolysis than suggested in our work, because such clearances would require a bearing mechanism which increases shear on the blood. The CFD model in this paper did not consider eccentric oscillations of the impeller.

Conclusion

This study investigated the effect of axial and radial clearance geometries on the hydrodynamic and haemolytic performance of a rotary centrifugal blood pump. The results from the present study show that incorporating very large clearances will not lead to minimised blood trauma. Although incorporating larger clearances in RBPs ensures that the shear stress acting on RBCs is reduced, the haemolysis level will eventually increase, due to a significant change in secondary flow rate, which consequently affects the RBC exposure time. In addition further decreasing the clearance size will adversely affect the hydraulic efficiency incorporating very small radial clearances may increase the risk of RBC damage due to excessive shear stress, while large clearances can cause high exposure time which may lead to the creation of large-scale stagnant vortices, which not only adversely affect the rotor stability of the impeller but also causes other blood complications. For all clearances in an RBP a compromise must be found between high shear stress at small clearances, and high secondary flow rate at large clearances. The main conclusion from this work, in which axial and radial clearances are assessed separately, is that the design of these two regions is inter-related. Axial and radial clearances must be designed simultaneously to prevent vortices in one or other region and allow laminar secondary flow. This is beneficial for both improving efficiency and reducing haemolysis.

Conflict of interest statement

None.

Acknowledgements

This report is independent research funded by the National Institute for Health Research [i4i, Turbocardia, II-LB-1111-20007]. Principal Investigator for the grant is Prof. T. Korakianitis. The views expressed in this publication

are those of the authors and not necessarily those of the NHS, the National Institute for Health Research or the Department of Health.

References:

1 . Lloyd-Jones, Donald, et al. "Heart disease and stroke statistics—2009 update." Circulation 119.3 (2009): e21-e181.
2 . Griffith, Bartley P., et al. "HeartMate II left ventricular assist system: from concept to first clinical use." The Annals of thoracic surgery 71.3 (2001): S116-S120.
3 . Christiansen, Stefan, Anna Klocke, and Rüdiger Autschbach. "Past, Present, and Future of Long-Term Mechanical Cardiac Support in Adults." Journal of cardiac surgery 23.6 (2008): 664-676.
4 . Rezaienia, Mohammad Amin, et al. "In vitro comparison of two different mechanical circulatory support devices installed in series and in parallel." Artificial organs 38.9 (2014): 800-809.
5 . Rezaienia, Mohammad Amin, et al. "Numerical and in vitro investigation of a novel mechanical circulatory support device installed in the descending aorta." Artificial organs 39.6 (2015): 502-513.
6 . Rezaienia, Mohammad Amin, et al. "In-vitro investigation of cerebral-perfusion effects of a rotary blood pump installed in the descending aorta." Journal of biomechanics 49.9 (2016): 1865-1872.
7 . Rezaienia, M. A., et al. "In-vitro investigation of the hemodynamic responses of the cerebral, coronary and renal circulations with a rotary blood pump installed in the descending aorta." Medical engineering & physics 40 (2017): 2-10.
8 . Okamoto, Eiji, et al. "Initial acute animal experiment using a new miniature axial flow pump in series with the natural heart." Artificial organs 39.8 (2015): 701-704.
9 . Wang, Yaxin, et al. "In vitro study of an intra-aortic VAD: effect of reverse-rotating mode on ventricular recovery." Engineering in Medicine and Biology Society (EMBC), 2015 37th Annual International Conference of the IEEE. IEEE, 2015.
10 . Fraser, Katharine H., et al. "A quantitative comparison of mechanical blood damage parameters in rotary ventricular assist devices: shear stress, exposure time and hemolysis index." Journal of biomechanical engineering134.8 (2012): 081002.
11 . Sibbald, Matthew, and Vladimír Džavík. "Severe hemolysis associated with use of the Impella LP 2.5 mechanical assist device." Catheterization and Cardiovascular Interventions 80.5 (2012): 840-844.
12 . Jennings, Douglas L., and Phillip A. Weeks. "Thrombosis in Continuous-Flow Left Ventricular Assist Devices: Pathophysiology, Prevention, and Pharmacologic Management." Pharmacotherapy: The Journal of Human Pharmacology and Drug Therapy 35.1 (2015): 79-98.
13 . Meyer, Anna L., et al. "Acquired von Willebrand syndrome in patients with a centrifugal or axial continuous flow left ventricular assist device." JACC: Heart Failure 2.2 (2014): 141-145.
14 . Myers, Timothy J., Tehreen Khan, and O. H. Frazier. "Infectious complications associated with ventricular assist systems." ASAIO journal46.6 (2000): S28-S36.
15 . Carswell, Dave, et al. "Development of a radial ventricular assist device using numerical predictions and experimental haemolysis." Medical engineering & physics 35.8 (2013): 1197-1203.
16 . Blackshear Jr, Perry L., Frank D. Dorman, and Joseph H. Steinbach. "Some mechanical effects that influence hemolysis." (1965): 112-117.
17 . Graefe, Roland, Andreas Henseler, and Ulrich Steinseifer. "Multivariate assessment of the effect of pump design and pump gap design parameters on blood trauma." Artificial organs 40.6 (2016): 568-576.
18 . Kosaka, Ryo, et al. "Effect of a bearing gap on hemolytic property in a hydrodynamically levitated centrifugal blood pump with a semi-open impeller." Bio-medical materials and engineering 23.1-2 (2013): 37-47.
19 . Kido, Kazuyuki, et al. "Computational fluid dynamics analysis of the pediatric tiny centrifugal blood pump (TinyPump)." Artificial organs 30.5 (2006): 392-399.
20 . Wu, Jingchun, et al. "Computational fluid dynamics analysis of blade tip clearances on hemodynamic performance and blood damage in a centrifugal ventricular assist device." Artificial organs 34.5 (2010): 402-411.
21 . James, Natalie L., et al. "Evaluation of hemolysis in the VentrAssist implantable rotary blood pump." Artificial organs 27.1 (2003): 108-113.

22 . Paul, Gordon, et al. "Slip and turbulence phenomena in journal bearings with application to implantable rotary blood pumps." Tribology International 104 (2016): 157-165.
23 . Watterson, Peter A., et al. "VentrAssist hydrodynamically suspended, open, centrifugal blood pump." Artificial Organs 24.6 (2000): 475-477.
24 . Thamsen, Bente, et al. "Numerical analysis of blood damage potential of the HeartMate II and HeartWare HVAD rotary blood pumps." Artificial organs39.8 (2015): 651-659.
25 . Bourque, Kevin, et al. "HeartMate III: pump design for a centrifugal LVAD with a magnetically levitated rotor." ASAIO journal 47.4 (2001): 401-405.
26 . Taskin, M. Ertan, et al. "Design optimization of a wearable artificial pump-lung device with computational modeling." Journal of Medical Devices 6.3 (2012): 031009.
27 . Paul, Gordon, et al. "Machinability and Optimization of Shrouded Centrifugal Impellers for Implantable Blood Pumps." Journal of Medical Devices 11.2 (2017): 021005.
28 . LaRose, Jeffrey A., et al. "Design concepts and principle of operation of the HeartWare ventricular assist system." ASAIO Journal 56.4 (2010): 285-289.
29 . Farrar, David J., et al. "Design features, developmental status, and experimental results with the Heartmate III centrifugal left ventricular assist system with a magnetically levitated rotor." ASAIO journal 53.3 (2007): 310-315.
30 . Korakianitis, Theodosios, et al. "Optimization of centrifugal pump characteristic dimensions for mechanical circulatory support devices." ASAIO journal 62.5 (2016): 545-551.
31 . Mozafari, Sahand, et al. "The Effect of Geometry on the Efficiency and Hemolysis of Centrifugal Implantable Blood Pumps." Asaio Journal 63.1 (2017): 53-59.
32 . Final HM III (presented by Dr. Walter Dembitsky at ISRBP 2015)
33 . Versteeg, Henk Kaarle, and Weeratunge Malalasekera. An introduction to computational fluid dynamics: the finite volume method. Pearson Education, 2007.
34 . Taskin, M. Ertan, et al. "Computational characterization of flow and hemolytic performance of the UltraMag blood pump for circulatory support." Artificial organs 34.12 (2010): 1099-1113.
35 . Granet, I. Fluid Mechanics. Prentice Hall, 1996.
36 . Kravchenko, Arthur G., Haecheon Choi, and Parviz Moin. "On the relation of near-wall streamwise vortices to wall skin friction in turbulent boundary layers." Physics of Fluids A: Fluid Dynamics 5.12 (1993): 3307-3309.
37. Guo, Shuangxi, and Wanping Li. "The Effect of Near-Wall Vortices on Wall Shear Stress in Turbulent Boundary Layers." Engineering 2.03 (2010): 190.
38 . Song, Xinwei, et al. "Computational fluid dynamics prediction of blood damage in a centrifugal pump." Artificial organs 27.10 (2003): 938-941.
39 . Paul, Gordon, et al. "The effects of ambulatory accelerations on the stability of a magnetically suspended impeller for an implantable blood pump." Artificial organs 40.9 (2016): 867-876.
40. Chan, W. K., et al. "Numerical investigation of the effect of blade geometry on blood trauma in a centrifugal blood pump." Artificial organs 26.9 (2002): 785-793.